J. Phys. Chem. A **2005,** *109,* 7489−7499

Potential Energy Surfaces, Product Distributions and Thermal Rate Coefficients of the Reaction of $O(^3P)$ with $C_2H_4(X^1A_g)$: A Comprehensive Theoretical Study

Thanh Lam Nguyen, Luc Vereecken, Xin Juan Hou, Minh Tho Nguyen,* and Jozef Peeters*

Department of Chemistry, University of Leuven, Celestijnenlaan 200F, B-3001 Leuven, Belgium

Received: June 3, 2005; In Final Form: June 28, 2005

The potential energy surface for the $O(^3P) + C_2H_4$ reaction, which plays an important role in C_2H_4/O_2 flames and in hydrocarbon combustion in general, was theoretically reinvestigated using various quantum chemical methods, including G3, CBS-QB3, G2M(CC,MP2), and MRCI. The energy surfaces of both the lowest-lying triplet and singlet electronic states were constructed. The primary product distribution for the multiwell multichannel reaction was then determined by RRKM statistical rate theory and weak-collision master equation analysis using the exact stochastic simulation method. Intersystem crossing of the "hot" CH_2CH_2O triplet adduct to the singlet surface, shown to account for about half of the products, was estimated to proceed at a rate of $\approx 1.5 \times 10^{11}$ s^{-1}. In addition, the thermal rate coefficients $k(O + C_2H_4)$ in the $T = 200-2000$ K range were computed using multistate transition state theory and fitted by a modified Arrhenius expression as $k(T) = 1.69 \times 10^{-16} \times T^{1.66} \times \exp(-331\ K/T)$. Our computed rates and product distributions agree well with the available experimental results. Product yields are found to show a monotonic dependence on temperature. The major products (with predicted yields at $T = 300$ K/2000 K) are: $CH_3 + CHO$ (48/37%), $H + CH_2CHO$ (40/19%), and $CH_2(X^3B_1) + H_2CO$ (5/29%), whereas $H + CH_3CO$, $H_2 + H_2CCO$, and $CH_4 + CO$ are all minor ($\leq$5%).

I. Introduction

The electrophilic addition reaction of the oxygen atom $O(^3P)$ with the simplest alkene, C_2H_4, is an attractive subject for both experimental and theoretical studies. There are some interesting reasons for reinvestigating this reaction: (i) the $O(^3P) + C_2H_4$ reaction not only plays an important role in the C_2H_4/O_2 flame,[1−3] but also in combustion chemistry in general because C_2H_4 is a key intermediate in the oxidation of methane and of larger hydrocarbons;[4−6] (ii) it is thought to be also of some importance in some cases for photochemical air pollution;[7] (iii) this reaction is of fundamental importance in chemical kinetics and challenging to theoretical chemists because of its complicated reaction mechanism.

Since the early 1950s, Cvetanovic and co-workers[8−13] carried out pioneering studies of the reactions of oxygen atoms with olefins in the gas phase.[8−13] A general reaction mechanism was suggested and summarized in three major steps.[7] First, oxygen atoms in their triplet ground electronic state undergo an electrophilic addition onto the C═C bond, forming adducts that are vibrationally excited triplet biradicals corresponding to the spin-conservation rule. Second, the triplet biradicals either decompose to products (by H- or CH_2- loss) or carry out intersystem crossing (ISC) to singlet biradicals. The first direct evidence for important H production from $C_2H_4 + O$ was provided by Ravishankara et al.[14] The triplet biradicals might also isomerize by a H migration, but this process was found to face a large barrier height[15,16] and cannot, therefore, compete with the direct decomposition. Finally, the singlet biradicals produced from the triplet adducts upon ISC may either convert to "hot" epoxides by ring closure or rearrange by internal migration of H atoms or alkyl groups into "hot" carbonyl compounds. These "hot" compounds may then either undergo collisional stabilization under high-pressure reaction conditions[17,18] or dissociate rapidly to various products under low-pressure conditions such as in molecular beam experiments.[19]

Earlier, one of the present authors used discharge-flow techniques in combination with molecular beam mass spectrometry to measure the thermal rate coefficients of the $O(^3P) + C_2H_4$ reaction at different temperatures under low-pressure conditions (0.5−5 Torr He) and to determine the primary product distributions for this reaction at 0.7−5 Torr He and T = 287−607 K.[20,21,23] The observed room-temperature rate constant was $(6.7 \pm 1) \times 10^{-13}$ cm^3 $molecule^{-1}$ s^{-1}, close to the present literature recommendation[22] of 7.5×10^{-13} cm^3 $molecule^{-1}$ s^{-1}. The product distribution results were: 48 ± 10% for $CH_3 + CHO$, 38 ± 10% for $CH_2CHO + H$, 10 ± 5% for $H_2CO + CH_2(X^3B_1)$, and 4% for $H_2CCO + H_2$; the observed yields showed only a slight pressure dependence, and the influence of temperature within this range was also found to be small. The results agreed well with the product distribution at room temperature reported previously by Endo et al.[24]

The major possible primary product channels of the $O(^3P) + C_2H_4$ reaction are presented below. Where possible, experimental reaction enthalpies[25] ($\Delta_r H$(0 K), in kcal/mol) are given, while the values in parentheses are obtained by using quantum chemical calculations (see next section).

---

* Corresponding authors. E-mail: Jozef.Peeters@chem.kuleuven.ac.be (J.P.); Minh.Nguyen@chem.kuleuven.ac.be (M.T.N.). Fax: int-32-16-327992.

10.1021/jp052970k CCC: $30.25 © 2005 American Chemical Society
Published on Web 08/04/2005

$$O(^3P) + C_2H_4(X^1A_g) \rightarrow CH_2CHO(X^2A'') + H(^2S) \quad (-17.0) \tag{1}$$

$$O(^3P) + C_2H_4(X^1A_g) \rightarrow H_2CO(X^1A_1) + CH_2(X^3B_1) \quad -5.4\ (-6.6) \tag{2}$$

$$O(^3P) + C_2H_4(X^1A_g) \rightarrow CH_3(X^2A_2'') + HCO(X^2A') \quad -27.9\ (-28.8) \tag{3}$$

$$O(^3P) + C_2H_4(X^1A_g) \rightarrow H_2CCO(X^1A_1) + H_2(X^1\Sigma_g) \quad -84.2\ (-85.1) \tag{4}$$

$$O(^3P) + C_2H_4(X^1A_g) \rightarrow CH_3CO(X^2A') + H(^2S) \quad (-23.5) \tag{5}$$

$$O(^3P) + C_2H_4(X^1A_g) \rightarrow CH_4(X^1A_1) + CO(X^1\Sigma^+) \quad -116.7\ (-117.4) \tag{6}$$

$$O(^3P) + C_2H_4(X^1A_g) \rightarrow \text{oxirane}(X^1A_1) \quad -83.2\ (-83.4) \tag{7}$$

$$O(^3P) + C_2H_4(X^1A_g) \rightarrow CH_3CHO(X^1A') \quad -111.9\ (-110.8) \tag{8}$$

$$O(^3P) + C_2H_4(X^1A_g) \rightarrow CH_2CHOH(X^1A') \quad -100.1\ (-100.7) \tag{9}$$

Some results of primary product distributions recently obtained under low-pressure conditions are collected in Table 1. It is believed[7] that the products ($CH_2CHO(X^2A'')$ + $H(^2S)$ and $H_2CO(X^1A_1)$ + $CH_2(X^3B_1)$) produced in channels (1) and (2) mainly arise from the triplet electronic surface, whereas the other products channels result from the singlet electronic state. Table 1 shows that, at room temperature, there are two major reaction channels (1) and (3), which produce $CH_2CHO(X^2A'')$ + $H(^2S)$ and $CH_3(X^2A_2'')$ + $HCO(X^2A')$, respectively, and contribute up to about 90% of the products. The remaining 10% is mainly accounted for by the products $H_2CO(X^1A_1)$ + $CH_2(X^3B_1)$, while other channels are minor.

At high pressures, P = 5−50 bar, substantial yields of acetaldehyde and oxirane from channels (7) and (8) were observed.[18] In addition, vinyl alcohol produced from channel (9) was detected in solid argon.[17] These results show that acetaldehyde, oxirane, and vinyl alcohol play a role as (key) intermediates in the $O(^3P)$ + C_2H_4 reaction.

The $O(^3P)$ + C_2H_4 reaction has been extensively studied using quantum chemical calculations. Yamaguchi et al.[26] used the UHF/4-31G level of theory to optimize geometries for several low-lying biradical states of the ring-opened oxirane ($^\bullet CH_2CH_2O^\bullet$). Yamaguchi[27] then refined their previous calculations and extensively explored the potential energy surface by using the projected perturbation method PMP2/6-31G(d)//UHF/6-31G(d). Dupuis et al.[28] characterized some stationary points for the electrophilic addition of $O(^3P)$ to the C=C bond of ethylene using multiconfiguration Hartree−Fock calculations. Although lower levels of theory were used at that time, the results obtained from these calculations were important and useful to qualitatively elucidate the reaction mechanism.[27,28] Most of the major channels on the triplet energy surface were theoretically investigated by Melius[15] using the BAC-MP4 theory and recently characterized in detail by Jursic[16] using the high level CBS-Q method. Some important results arisen from these calculations are: (i) the H-abstraction channel from C_2H_4 by $O(^3P)$, leading to $OH(X^2\Pi)$ + $C_2H_3(X^2A')$, faces a barrier of 10.4 kcal/mol, much higher than that of the addition step (0.4 kcal/mol), such that the former cannot compete with the latter at low and fairly high temperature; (ii) the triplet biradical adduct formed from the addition step rapidly decomposes into CH_2CHO + H, facing a barrier of only 15.3 kcal/mol; and (iii) the 1,2-H migration in this adduct faces a high energy barrier of 28.1 kcal/mol, and is therefore not relevant.

In the singlet electronic state, unimolecular rearrangements connecting acetaldehyde, hydroxyethylidene (CH_3−C−OH), and vinyl alcohol, followed by their thermal decompositions to various products, were computed using G1 theory by Smith et al.[29]

As far as we are aware, previous theoretical calculations have, however, not been used to address the product distributions and/or thermal rate coefficients of the $O(^3P)$ + C_2H_4 reaction. Considering its important role in combustion chemistry as well as its fundamental kinetic interest, we set out to reinvestigate this reaction using different higher levels of theory such as the G3,[30] CBS-QB3,[31] G2M(CC,MP2),[32] and MRCI methods.[33,34] We have constructed the potential energy surfaces of the lowest-lying triplet and singlet electronic states. Particular attention has been paid to the product distributions and thermal rates, which were computed on the basis of the information gained from the potential energy surfaces (zero-point energy corrected potential energies, harmonic vibration frequencies, and rotational constants). We also addressed the intriguingly fast triplet → singlet ISC crossing that bears heavily on the product makeup.

II. Theoretical Approaches

II.1. Quantum Chemical Calculations. Local minima and transition structures (TS) on the potential energy surface (PES) were initially optimized using density functional theory with the hybrid B3LYP[35,36] functional in conjunction with the 6-311++G(3df,2p) basis set.[37] Analytical harmonic vibration frequencies were computed at this level in order to verify the character of the stationary points located (one imaginary frequency for a TS and all real frequencies for a minimum). Zero-point energies were used unscaled to correct the relative energies. To obtain more accurate relative energies, the G2M(CC,MP2)[32] method was used to compute single-point electronic energies based on the B3LYP/6-311++G(3df,2p) optimized geometries. Additionally, the CBS-QB3[31] and G3[30] methods were also used. The values computed at the G2M(CC,MP2), CBS-QB3, and G3 levels are in good agreement with each other, within 1−2 kcal/mol, and with available experimental data (see Table 2). In this paper, unless otherwise mentioned, we adopt the average of the values computed at the last three theoretical levels for the subsequent kinetic analyses. Our averaged values also agree well with those reported in the literature using the G1[29] and CBS-Q theory.[16]

There are several stationary points of which the wave functions possess a two-reference character (see Table 3). In these cases, the multiconfiguration CASSCF(8,8) method,[38,39] in combination with the correlation consistent cc-pVDZ basis set,[37] was used to re-optimize geometries and to perform analytical Hessian calculations. The relevant energies were then refined by including dynamic electronic correlations using the multireference internally contracted single- and double-excitation configuration interaction method (hereafter denoted as MR-CI)[33,34] in combination with a larger extended cc-pVTZ basis set.[37] The quadruple correction (Q) by Davidson's scheme[40] was also included to overcome the size-consistency problem in a truncated CI. For a set of constrained optimizations with fixed C−O bond distances or fixed CCO angles (see below), the CASSCF(8,8)/cc-pVDZ method was employed, and the energies

TABLE 1: Primary Products Distribution for the O(^{3}P) + C_2H_4(X^1A_g) Reaction Observed Under Low-Pressure Conditions

authors, year, reference	channel (1)	channel (2)	channel (3)	channel (4)	channel (5)	ratio[a]
Endo et al. (1986), ref 24	40 ± 10%	10 ± 5%	50 ± 10%			50:50
Peeters et al. (1988), ref 23	38 ± 10%	10 ± 5%	48 ± 10%	4%		48:52
Bley et al. (1988), ref 18	50 ± 10%	6 ± 3%	44 ± 10%			56:44
Koda et al. (1991), ref 75	46 ± 15%		54 ± 15%			46:54
Matsui et al. (2004), ref 76	47 ± 4%		53 ± 4%			47:53
Casavecchia et al. (2004), ref 65	27 ± 6%	16 ± 8%	43 ± 11%	13 ± 3%	1 ± 0.5%	≈43:57
YT Lee et al. (1989), ref 19 C_2D_4 + O reaction	(29 ± 25%)		(71 ± 25%)			≈30:70[b]

[a] Ratio of yields from the triplet surface over those from the singlet surface as follows from our theoretical analysis (see text). [b] Measured for C_2D_4 + O.

TABLE 2: Calculated Relative Energies[a] (kcal/mol, $T = 0$ K) for Various Species in the O(^{3}P) + C_2H_4(X^1A_g) Reaction Using Different Levels of Theory

species	B3LYP[b]	G2M	CBS-QB3	G3	average[c]	exp.[d]	G1[f]	CBS-Q[g]
O(X^3P) + C_2H_4(X^1A_g)	0.0	0.0	0.0	0.0	0.0	0.0		0.0
CH_2(X^3B_1) + H_2CO(X^1A_1)	−7.9	−7.0	−6.1	−6.8	−6.6	−5.4		
CH_2($^1A_1$) + H_2CO(X^1A_1)	3.0	2.5	1.8	2.7	2.3	3.6		
H(X^2S) + H_2CCHO(X^2A'')	−19.7	−16.7	−17.8	−16.5	−17.0		−15.2	−17.4
H(X^2S) + CH_3CO(X^2A')	−25.2	−24.0	−23.6	−22.8	−23.5		−22.1	−24.4
H(X^2S) + CH_3(X^2A_2'') + CO($X^1\Sigma^+$)	−13.1	−16.2	−14.0	−14.6	−14.9	−13.4	−14.0	−15.4
CH_3(X^2A_2”) + CHO(X^2A')	−33.2	−28.8	−28.4	−29.1	−28.8	−27.9	−26.7	−29.7
H_2CCO(X^1A_1) +H_2($X^1\Sigma_g$)	−87.8	−83.9	−86.3	−85.2	−85.1	−84.2		
HC°COH(X^1A') + H_2($X^1\Sigma_g$)	−50.7	−49.3	−52.6	−51.0	−51.0			
CO($X^1\Sigma^+$) + CH_4(X^1A_1)	−114.7	−117.3	−117.8	−117.1	−117.4	−116.7	−117.7	
OH($X^2\Pi$) + C_2H_3(X^2A')	3.8	8.8	7.3	6.5	7.5	8.3	10.6	7.2
°O−CH_2-°CH_2(^3A), **Int1a**	−29.3	−23.6	−24.4	−24.0	−24.0 (−24.0)			−24.4
°O−CH_2-°CH_2($^3A'$), **Int1b**	−23.2	−18.3	−17.2	−19.3	−18.3			
CH_3CHO(^3A), **Int2**	−38.4	−32.1	−32.8	−32.2	−32.4			−32.9
CH_2CHOH(^3A), **Int3**	−37.6	−32.9	−34.0	−34.0	−33.7			−33.6
°O−CH_2-°CH_2(^1A), **Int4**	−34.4	−24.0	−22.7	−21.2	−22.6 (−25.9)			
CH_3CHO(X^1A'), **Int5**	−110.4	−109.8	−111.8	−110.7	−110.8	−111.9	−110.8	
oxirane(X^1A_1), **Int6**	−81.4	−82.5	−84.7	−82.9	−83.4	−83.2		
CH_2CHOH-a(X^1A'), **Int7a**	−99.8	−98.5	−101.2	−100.4	−100.1	−100.7		
CH_2CHOH-b($^1A'$), **Int7b**	−98.8	−97.6	−100.3	−99.5	−99.1		−99.6	
CH_3COH-a(X^1A'), **Int8a**	−59.4	−59.1	−60.4	−59.8	−59.8		−59.9	
CH_3COH-b($^1A'$), **Int8b**	−56.9	−56.1						
CH_3OCH(^1A), **Int9**	−42.9	−43.1	−44.0	−43.2	−43.5			
CH_3OCH(^3A)	−18.8	−15.7						
TS1a($^3A''$)		2.8	1.0		1.9			0.4
TS1b($^3A'$)	−2.3	3.8	2.2	1.9	2.6			
TS2a($^3A''$	3.8	12.8	9.6	10.5	11.0			10.4
TS2b($^3A'$)	4.5	13.6	10.1	11.1	11.6			
TS3(^3A)	−13.8	−7.6	−9.9	−8.5	−8.7			
TS4(^3A)	−4.7	−1.5	−2.4	−1.6	−1.9			
TS5(^3A)	−0.2	8.2	6.3	8.1	7.5			6.4
TS6(^3A)	0.1	5.6	4.1	4.7	4.8			3.7
TS7(^3A)	−25.8	−19.0	−19.1	−20.5	−19.6			−22.3
TS8(^3A)	−18.5	−14.5	−14.1	−16.3	−15.0			−17.9
TS9(^3A)	−0.5	9.3	7.2	7.4	8.0			
TS10(^1A)					(−28.4)			
TS11(^1A)	−30.4	−22.3	−24.8	−17.5	−21.5 (−24.3)			
TS12(^1A)					(−25.9)			
TS13(^1A)	−20.8	−18.4	−19.3	−18.3	−18.6 (−24.5)			
TS14(^1A)	−44.6	−42.2	−44.1	−43.2	−43.2		−43.4	
TS15($^1A'$)	−31.1	−30.6	−31.9	−31.5	−31.4		−31.7	
TS16(^1A)	−37.5	−35.9	−37.4	−36.6	−36.6		−36.5	
TS17(^1A)[e])	−41.1	−34.7	−37.8	−34.7	−35.4			
TS18(^1A)[e])	−30.7	−26.6	−25.0	−25.2	−25.6			
TS19(^1A)[e])	−23.1	−18.9	−16.7	−18.5	−18.0			
TS20(^1A)	−33.3	−28.8	−30.6	−29.1	−29.5		−29.8	
TS21(^1A)	−30.1	−26.7	−28.0	−27.6	−27.4		−27.9	
TS22(^1A)	−11.5	−12.9	−14.2	−13.9	−13.7			
TS23(^1A)	−6.4	−7.6	−8.6	−6.5	−7.6			
TS24($^1A'$)	−18.0	−13.4	−15.6	−14.6	−14.5			
TS25($^1A'$)	−28.2	−25.8	−27.5	−27.1	−26.8			

[a] Values in the parentheses obtained at the CASSCF(8,8)/MR−CISD+Q(8,8) level. [b] B3LYP stands for the B3LYP/6-311++G(3df,2p) level. [c] Average = $(\Delta E_{G2M} + \Delta E_{CBS-QB3} + \Delta E_{G3})/3$ [d] Experimental values (at $T = 0$ K) are taken from the webpage: http://srdata.nist.gov/cccbdb/. [e] Microvariational transition states. [f] ref 29. [g] ref 16.

were then improved by including dynamic electronic correlations using the multireference perturbation theory, CASPT2(8,8)/cc-pVDZ.[41,42]

The DFT-B3LYP, G2M(CC,MP2), CBS-QB3, and G3 calculations were performed using the Gaussian 03 package;[43] the CASSCF geometries and vibrational frequencies were computed

TABLE 3: Computed Two Most Important CI coefficients (C_1 and C_2) for Wave Functions of Various Stationary Points Using the CASSCF(8,8)/cc-pVDZ Level of Theory

structure	C_1	C_2
Int4	−0.80928624	0.56130081
TS10	0.85525651	−0.47847802
TS11	0.80533897	−0.56843161
TS12	−0.88994747	0.40236129
TS13	0.79640488	−0.57531866

using the Dalton package;[44] and the CASSCF constrained optimizations, CASPT2, and MRCI energies were carried out using Molpro 2002.[45] To simplify the presentation of data, all optimized geometries, harmonic vibration frequencies, rotational constants, and energies are given in the Supporting Information.

II.2. RRKM/Master Equation Calculations. According to the statistical RRKM theory of unimolecular reaction rates,[46−51] the microcanonical rate constant $k(E)$ for a reactant with internal energy E can be expressed as:

$$k(E) = \frac{\alpha}{h} \times \frac{G^{\ddagger}(E - E^{\ddagger})}{\rho(E)} \tag{10}$$

where α is the reaction pathway degeneracy, h Planck's constant, $E^{\ddagger}$ the relative energy of the TS, $G^{\ddagger}(E - E^{\ddagger})$ the sum of internal states of the transition structure (TS) for energies up to $E - E^{\ddagger}$ and $\rho(E)$ the density of internal states for a reactant molecule with internal energy E.

The chemically activated $CH_3CHO(X^1A')$ intermediate can dissociate into $CH_3 + CHO$, $H + CH_2CHO$, or $H + CH_3CO$, all three without exit barrier. For these channels, variational transition state theory[48−51] was used to locate the kinetic bottleneck. For this purpose, first, the UB3LYP/6-311++G(3df,2p) level of theory was employed to optimize geometries and calculate vibration frequencies along the reaction coordinate (RC) by constrained optimizations with fixed C−C or C−H bond lengths in $CH_3CHO(X^1A')$. The total energies along the RC were then refined by single-point electronic energy calculations at the G2M level. Using the resulting PES, the $k(E)$ at every position along the RC were computed for an internal CH_3CHO energy E of 110.8 kcal/mol, corresponding to the decrease in potential energy relative to the reactants (see Figs S6, S7, and S8 in Supporting Information). The minimal $k(E)$ were found for bond distances of 2.7 Å for the C−C bond, 2.6 Å for C−H in the CH_3 group, and 2.7 Å for C−H in the CHO group, respectively. The characteristics at these points along the RCs will be used in the subsequent kinetic calculations.

It should be noted that, for the $CH_3CHO(X^1A') \rightarrow CH_3(X^2A_2'') + CHO(X^2A')$ channel, one internal degree of freedom of the CH_3 group in the CH_3CHO molecule and in the variational transition structures corresponds to a hindered internal rotation around the C−C axis. This mode was projected out and treated appropriately as a one-dimensional hindered internal rotation, having an approximate potential energy function

$$V = \frac{V_o}{2}(1 - \cos \sigma x) \tag{11}$$

where V_o is the classical barrier height of internal rotation, $\sigma = 3$ the rotational symmetry number, and x the internal rotation angle. Therefore, the sum and density of states in eq 10 are now taken as the convolution of the density of the one-dimensional hindered internal rotor with the sum and density of states of the vibration levels:[48,51]

$$k(E) = \frac{\alpha}{h} \times \frac{\int_0^{E-E^{\ddagger}} G_v^{\ddagger}(E - E^{\ddagger}) - x\rho_{hr}^{\ddagger}(x)dx}{\int_0^{E} \rho_v(E - y)\rho_{hr}(y)dy} \tag{12}$$

where ρ_{hr} is the density of states of the one-dimensional hindered internal rotor which can be either directly counted if E_{int} (internal energy) $\leq 10 \times V_o$ based on the first 50 internal rotation energy levels gained by solving the one-dimensional Schrödinger equation[52,53] or approximately computed using an analytical formula derived by Knyazev[54] for classical one-dimensional hindered internal rotations if $E_{int} > 10 \times V_o$. Input parameters required for these calculations are given in Table 4. The Beyer−Swinehart−Stein−Rabinovitch algorithm[55,56] was used to compute the sum and density of states in eqs 10 and 12 employing a grain size of 1 cm^{-1}.

The product distributions for the $O(^3P) + C_2H_4$ reaction occurring on the (separate) triplet or singlet energy surfaces were obtained by solving the energy-grained master equations under various conditions ($P = 5−760$ Torr, $T = 287−2000$ K). The Lennard−Jones collision parameters for the bath gas He are $\sigma = 2.55$ Å and $\epsilon/k_B = 10$ K while those for $[C_2H_4O]$ species are taken to be $\sigma = 4.08$ Å and $\epsilon/k_B = 421$ K, i.e., similar to those of ethylene oxide.[57] The collision frequency Z_{LJ} $[M]$ was computed to be 1.1×10^{10} s^{-1} at 1 atm and room temperature. The probability density function for collisional energy transfer was computed, adopting the biexponential model of Troe.[58] An average energy transferred per collision $\langle \Delta E \rangle_{all}$ of -130 cm^{-1} was chosen.[57]

In the energy-grained master equation, the maximum energy considered was 200 kcal/mol above the lowest conformer (e.g., $CH_3CHO(X^1A')$), and a very small energy band size of 0.03 kcal/mol was chosen to ensure that the density of states does not change significantly within one band. A stochastic simulation is used to solve the master equation following Gillespie's exact stochastic algorithm.[59−61] To obtain products distributions with high precision, a large number of trials was chosen, about 10^7. The choice of a good random number generator is very important in the stochastic simulation; in this application, the Mersenne Twister (MT19937) random number generator was chosen.[62] A detailed explanation on the stochastic solution of the master equation was given in our earlier paper.[63]

Additionally, we computed the primary products distribution under the collision-free conditions ($P \approx 0$ Torr) in molecular beam experiments (MBE). In particular, values at an internal energy of 12.9 kcal/mol above the initial reactants have been determined in order to compare with the recent MBE results of Casavecchia et al.[64−66]

III. Results and Discussion

III.1. Potential Energy Surfaces. *The Triplet Electronic State.* As a first reaction step, the $O(^3P)$ atom may either abstract a H atom or add onto a C atom of the $H_2C{=}CH_2$ molecule. These processes proceed on the triplet energy surface corresponding to the spin-conservation rule. H-abstraction from C_2H_4 by $O(^3P)$ proceeds via the asymmetric **TS2a**($^3A''$) as well as the symmetric **TS2b**($^3A'$), which both directly correlate to products $OH(X^2\Pi) + C_2H_3$ (of Figure 1). Both transition states have a high relative energy of about 11−12 kcal/mol above the initial reactants and ∼10 kcal/mol higher than that of the addition transition structures, such that abstraction cannot compete with addition at low to fairly high temperatures. Addition of $O(^3P)$ onto a C atom takes place via both **TS1a**($^3A''$) and **TS1b**($^3A'$), which lie only 1.3 and 2.6 kcal/mol above the initial reactants. These values agree well with the Arrhenius

TABLE 4: Computed Classical Barrier Height (V_o, in cm^{-1}) for the Internal Rotation of the CH$_3$ Group around the C−C Axis in CH$_3$CHO, Internal Rotation Constant (B, in cm^{-1}), Harmonic Vibration Frequency from the Hessian (in cm^{-1}) and Internal Rotation Frequency at the Potential Minimum (ω, in cm^{-1}) Using the UB3LYP/6-31G(d$_{5d}$,P) Level for the CH$_3$ Group in Various Configurations, Optimized at Fixed C−C Bond Distances, along the Reaction Coordinate of the CH$_3$CHO → CH$_3$ + CHO Channel

R_{C-C}[a]	V_o (cm^{-1})	harm. freq. (cm^{-1})	B (cm^{-1})[b]	ω (cm^{-1})[c]
CH$_3$CHO	404.5 [d])	156.5	6.33	151.8
2.0	63.7	92.4	6.09	59.1
2.1	44.0	83.4	6.06	49.0
2.2	31.4	75.3	6.03	41.3
2.3	21.4	68.6	6.01	34.0
2.4	15.0	61.8	5.99	28.4
2.5	11.0	56.6	5.97	24.3
2.6	8.9	49.9	5.93	21.8
2.7	7.8	41.7	5.90	20.4
2.8	6.3	31.8	5.89	18.3
2.9	5.3	18.9	5.88	16.7
3.0	4.2	13.9	5.86	14.9

[a] C−C bond distance (Å). [b] $B = h^2/(8\pi^2 I_{hr})$, with I_{hr} taken as $I_{CH3} \times I_{CHO}/(I_{CH3} + I_{CHO})$, where I_{CH3} and I_{CHO} are the moments of inertia of CH$_3$ and CHO rotating around the C−C axis, respectively. [c] $\omega = \sigma\sqrt{V_o B}$, where $\sigma = 3$ is the rotational symmetry number of the CH$_3$ group. [d] In good agreement with $V_o = 400$ cm^{-1} observed in experiment (ref 77).

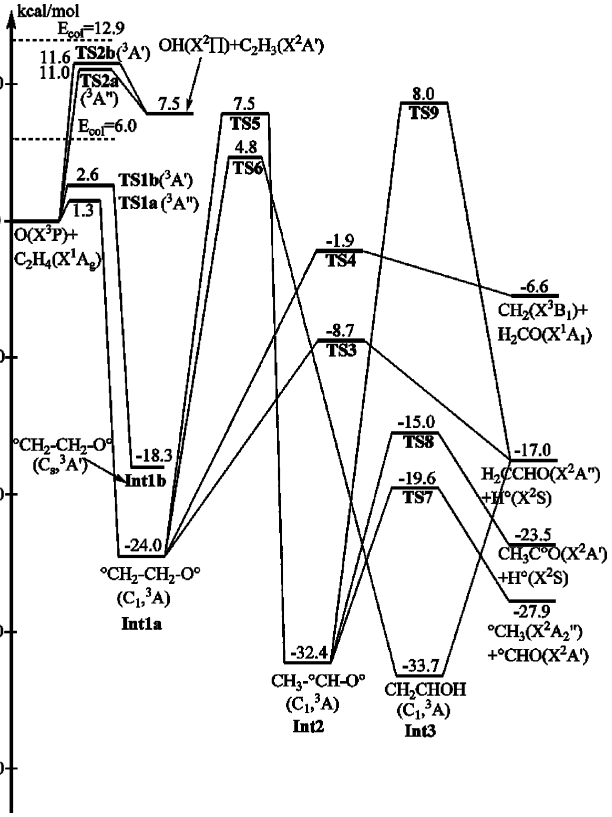

Figure 1. Triplet potential energy surface for the O(^{3}P) + C$_2$H$_4$ reaction based on the average relative energies computed at the G3, CBS-QB3, and G2M levels of theory.

activation energy of about 2 kcal/mol derived from experiment.[20−22,67] It should be indicated here that **TS1a** is a very early, reactant-like transition state and could not be located using B3LYP; we used the IRCMax[68] method to characterize this transition state (see Fig S9 in Supporting Information). The addition of O(^{3}P) via **TS1a** forms the triplet biradical $^{\bullet}$CH$_2$-CH$_2$O$^{\bullet}$(^{3}A) (hereafter denoted as **Int1a**), which lies 24.0 kcal/mol below the initial reactants, whereas that via **TS1b** leads to **Int1b**(^{3}A′), lying 18.3 kcal/mol below the reactants. It is expected that **Int1b**, after being formed, will undergo facile conversion by an internal rotation into **Int1a**. Because of the large energy difference, **Int1a** is expected to comprise the bulk of the **Int1** population, and the reactions of the **Int1b** form are not studied separately.

Starting at **Int1a**, there are four possible reaction pathways: (i) it can dissociate into the products CH$_2$CHO + H via **TS3** with a barrier height of 15.3 kcal/mol; (ii) **Int1a** can dissociate into products CH$_2$(X^{3}B$_1$) + H$_2$CO by breaking the C−C bond via **TS4**, facing a barrier of 22.1 kcal/mol; (iii) **Int1a** could undergo a 1,2-H shift**,** facing a high barrier of 31.5 kcal/mol (**TS5**) and leading to triplet CH$_3$CHO (**Int2**); and finally, (iv) **Int1a** could isomerize to triplet CH$_2$CHOH by 1,2-H migration over a high barrier of 28.8 kcal/mol (**TS6**). Clearly, the lower-barrier dissociation reactions will far outrun the isomerizations. Because, moreover, the isomerization TSs lie even above the entrance transition states, it is justified to neglect these steps in our kinetic analysis in the next section.

Triplet CH$_3$CHO **Int2**, if formed, can decompose via three different channels, of which the channel via **TS7** leading to CH$_3$ + CHO is predominant because of its lower barrier height of 12.8 kcal/mol. Triplet CH$_2$CHOH (**Int3**), being 33.7 kcal/mol below the initial reactants, will rapidly dissociate into products H$_2$CCHO + H without an exit barrier.

As can be seen from the discussion above and from Figure 1, the products CH$_2$(X^{3}B$_1$) + H$_2$CO and H$_2$CCHO + H are found to be major and predominant on the triplet energy surface, whereas CH$_3$ + CHO are expected to be minor products with yields ≤1%. However, the experimental data (Table 1) show that the yield of the products CH$_3$ + CHO is about 40−50% depending, on the experimental conditions. One must, therefore, conclude that the products CH$_3$ + CHO arise from the singlet electronic state after ISC from the triplet surface of the $^{\bullet}$CH$_2$-CH$_2$O$^{\bullet}$ biradical to the singlet surface, in agreement with the views of Cvetanovic et al.[7] Note that the ISC process at hand is not collision-induced because the product branching ratios are nearly insensitive to the pressure (from 30 mTorr to 760 Torr).[19] In addition, the products CH$_3$ + CHO were observed in molecular beam experiments under collision-free conditions previously by Lee et al.[19] and more recently by Casavecchia et al.[64−66]

Thus, it is of interest to theoretically investigate crossing seams, which are expected to lie close to the stationary points of both the triplet and singlet biradicals $^{\bullet}$CH$_2$CH$_2$O$^{\bullet}$. Note that the ratios of each of the harmonic vibration frequencies (except the internal rotation mode of the CH$_2$ group around the C−C axis) of the triplet and singlet biradicals computed at the CASSCF level are all close to unity, indicating that both energy surfaces are strongly parallel in the harmonic vibration space regions in these 3N-7 dimensions. To illustrate crossing seams, we chose the C−O stretching and the CCO bending coordinates (see Figure 2). First we carried out constrained optimizations at fixed C−O bond lengths or fixed CCO angles using the CASSCF(8,8)/cc-pVDZ level; energies were then refined using the CASPT2(8,8)/cc-pVDZ method. Figure 2a shows the addition path of O onto a C═C carbon, corresponding to the C−O stretching mode. After passing from the initial reactants through **TS1a** on the triplet surface, the triplet curve along the C−O stretching coordinate approaches the singlet curve, and they start overlapping at a C−O bond length of about 1.6 Å. Such crossing seams of the two energy surfaces are a space region lying close to the harmonic vibration region of the triplet biradical adduct. Figure 2b shows the bending path of the CCO

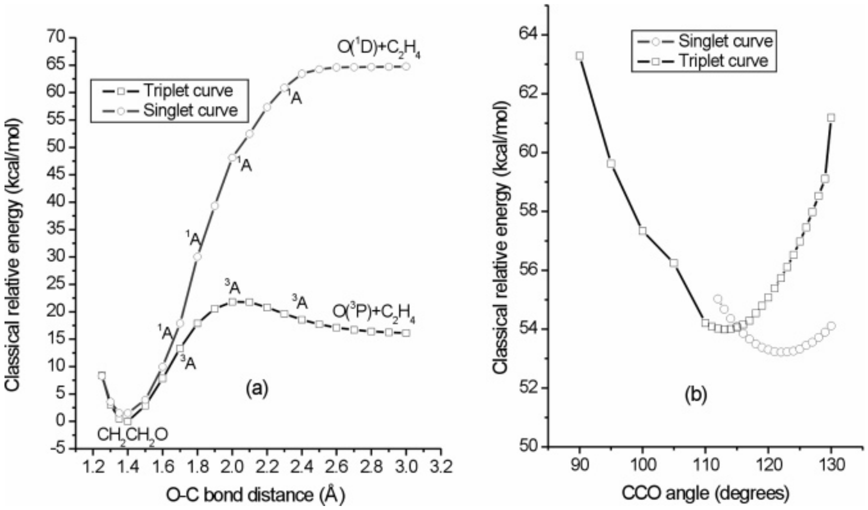

Figure 2. Crossing seams on the triplet and singlet energy surfaces computed at the CASPT2/CASSCF level: (a) for the C−O stretching coordinate and (b) for the CCO bending coordinate.

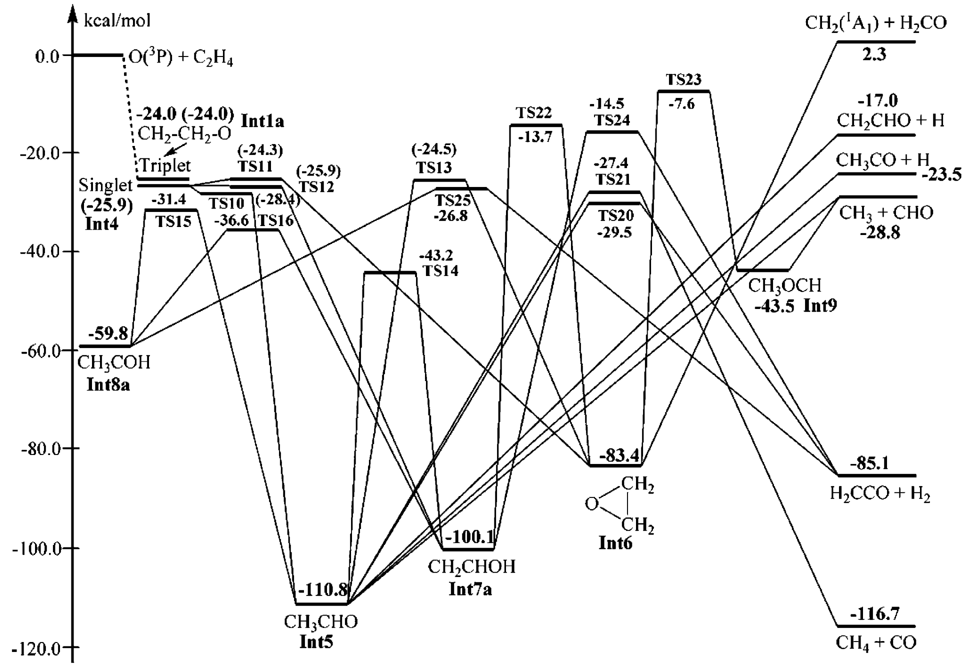

Figure 3. Singlet potential energy surface for the $O(^3P) + C_2H_4$ reaction based on the average relative energies computed at the G3, CBS-QB3, and G2M levels of theory. The values in parentheses are obtained at the MRCI level. The triplet entrance part is shown by dashed lines.

angle. The triplet and singlet curves almost overlap in the CCO angle range from 110 to 120°. It thus turns out that crossing seams are predicted to exist in the (3N-7)-dimensional space regions neighboring the stationary structure of the $^{\bullet}CH_2CH_2O^{\bullet}$-(^{3}A) biradical, such that high probabilities are expected for crossing from the triplet to the singlet surface. It should be emphasized that the ISC process considered here is one of a highly chemically activated species.

The Singlet Electronic State. The singlet biradical $^{\bullet}CH_2CH_2O^{\bullet}$ (denoted as **Int4**), produced by ISC from **Int1a**, lies 25.9 kcal/mol (computed at the MRCI method) below the initial reactants and only 1.9 kcal/mol lower than its triplet counterpart. Starting from **Int4**, there are three possible reaction pathways (see Figure 3), namely: (i) a 1,2-H migration leading to acetaldehyde CH_3CHO (**Int5**) via **TS10**; the small barrier of 0.5 kcal/mol at the CASSCF level disappears when using the MRCI level, indicating that **Int4** has a very short lifetime and isomerizes spontaneously to the singlet CH_3CHO; (ii) **Int4** ring-closure forming the oxirane (**Int6**) via **TS11** with a barrier height of 1.6 kcal/mol; and (iii) **Int4** isomerization to vinyl alcohol $CH_2{=}CHOH$ (**Int7a**) by a 1,2-H shift via **TS12**; this latter step is characterized as barrierless at the MRCI level.

Acetaldehyde (**Int5**) can isomerize to **Int6**, **Int7a**, and 1-hydroxyethylidene CH_3COH **Int8a** via **TS13**, **TS14**, and **TS15**, respectively. These steps face barriers of 86.3, 67.6, and 79.4 kcal/mol, respectively. **Int5** can also directly decompose into different products such as $CH_3 + CHO$ and $CH_3CO/CH_2CHO + H$ via loose, variational transition states without exit barriers or to $CH_2CO + H_2$ and $CH_4 + CO$ through tight transition structures with exit barriers. As a result, the product pair $CH_3 + CHO$ emerges as predominant, whereas the pair $CH_4 + CO$ is predicted as minor even though the latter product channel is thermodynamically the most favored, having indeed the largest reaction enthalpy of −116.7 kcal/mol.

Oxirane (**Int6**) can either isomerize (back) to **Int5**, to **Int7**, and to singlet carbene CH_3OCH via **TS13**, **TS22**, and **TS23**, respectively, or directly dissociate into products $CH_2(^1A_1) + H_2CO$ without exit barrier. As can be seen in Figure 3, the

TABLE 5: Computed Primary Products Distribution (%) Evolving from the Triplet $^{\bullet}CH_2CH_2O^{\bullet}$ Biradical on the Triplet Surface under Various Reaction Conditions

T (K)	P (Torr)	H + CH_2CHO	$CH_2(X^3B_1)$ + H_2CO	O + C_2H_4
287	5	88.7	11.3	0.0
	760	88.8	11.2	0.0
298	5	88.4	11.6	0.0
	760	88.5	11.5	0.0
500	5	81.5	18.4	0.1
	760	81.5	18.4	0.1
607	5	76.9	23.0	0.1
	760	76.9	23.0	0.1
1000	5	60.0	39.7	0.3
	760	60.0	39.7	0.3
1500	5	44.2	55.2	0.6
	760	44.2	55.2	0.6
2000	5	34.7	64.6	0.7
	760	34.7	64.6	0.7

isomerization of **Int6** back to **Int5** faces the lowest barrier, and accordingly, this step should predominate. Similar to **Int6**, the **Int7a** and **Int8a** species produced from the above-mentioned steps rapidly isomerize back to **Int5** via low-lying transition structures **TS14** and **TS15**. Direct H_2-elimination from **Int7a** and **Int8a** are also possible, leading to $CH_2CO + H_2$ via **TS24** and **TS25**. The latter TSs, however, lie substantially higher than **TS14**, **TS15** and **TS16**.

Overall, the theoretical results obtained for the singlet energy surface indicate that isomerization processes take place via transition structures that are lying low in energy, such that extensive internal rearrangements of the singlet [C_2H_4O] system should occur before final fragmentation to end products at low pressures or collisional stabilization at high pressures.

III.2. Product Distribution. *Temperature and Pressure Dependence.* The *partial* product distributions from the triplet and singlet $^{\bullet}CH_2CH_2O^{\bullet}$ adducts were derived separately by solving the appropriate master equations independently. The initial energy distribution of formation of the triplet $^{\bullet}CH_2CH_2O^{\bullet}$ adduct from O(^{3}P) + C_2H_4 via **TS1a** was derived from detailed balance considerations.[47] The results obtained under various reaction conditions ($T = 287-2000$ K and $P = 5-760$ Torr) are presented in Tables 5 and 6. They are independent of pressure over the range considered, but vary as a function of temperature. Our predictions agree well with the experimental observations (see Table 1). We performed some sample calculations at higher pressures to search the onset of the falloff region, but found only a small fraction of stabilization (<10%) even at 100 atm for combustion temperatures, T~1500 K. Hence, we will focus here on the aforementioned temperature and pressure region. For the triplet state, the yield of H + CH_2CHO from **Int1a** markedly decreases from 89% at 287 K to 35% at 2000 K, while the yield of $CH_2(X^3B_1) + H_2CO$ increases from 11% to 65%. The yield of collisionally stabilized triplet adduct is negligible even at $P = 760$ Torr, as the collision frequency of 10^{10} s^{-1} is much smaller than the combined rate of the decomposition channels ($\approx 1.3 \times 10^{11}$ s^{-1} at room temperature), and dozens of collisions are required to bring the adduct's total energy below the level of the lowest-lying decomposition TS. In fact, the triplet biradical barely loses any of its initial energy during its lifetime. Note, however, that the lifetime of the triplet adduct of about 8 ps should be long enough for quasistatistical distribution of the vibration energy over all modes. The fraction of adducts that redissociate back into the initial reactants is also small, <1%. It turns out that isomerization processes of the triplet adduct **Int1a** to **Int2** and **Int3** contribute less than 1% even at 2000 K because **TS5** and **TS6** lie much higher in energy than **TS1a** (see Figure 1).

For the singlet state, the calculated yield of collisionally stabilized [C_2H_4O] is similarly small and negligible. When the temperature increases from 287 to 2000 K, the yield of CH_3 + CHO drops considerably from 87% to 67%, while the yields of CH_3CO + H, CH_2CHO + H, $H_2 + H_2CCO$, and CH_4 + CO each increase to ≈5−10%.

Tables 5 and 6 show that H + CH_2CHO and $CH_2(X^3B_1) + H_2CO$ are major products from the triplet $^{\bullet}CH_2CH_2O^{\bullet}$ adduct, whereas the singlet adduct yields predominantly CH_3 + CHO. To compute the overall product distribution from the *partial*, separate data obtained above, the intersystem crossing between the triplet and singlet energy surfaces must be taken into account, in competition with the chemically activated reactions of the adducts. Thus, information is needed on the ISC rates at the crossing seams of the two energy surfaces. To compute these rates, trajectory dynamic calculations, e.g., "on the fly" nonadiabatic dynamics,[69,70] are certainly required. However, such calculations are far beyond the scope of this study. Here, we will proceed in a different way: making use of the rates of the unimolecular reactions derived from RRKM theory, we will estimate the ISC rate based on the experimentally observed *overall* primary products (collected in Table 1).

Our theoretical results clearly show that the products CH_2CHO + H and $H_2CO + CH_2(X^3B_1)$ of channels (1) and (2) arise from the triplet electronic surface, whereas the other product channels can only result from the singlet electronic state. Combining this with the experimental product yields presented in Table 1, one has to conclude a ratio for total triplet and total singlet yields of about 45% versus 55%, with an uncertainty margin of 5% each.

Another question that remains open is whether the crossing rates and their ratio depend on internal energy. According to previous experiments carried out by us,[23] and always in the light of the present theoretical findings, the ratio for triplet yields and singlet yields is only weakly dependent on temperature, its value barely changing from 45:55 at 287 K to 43:57 at 607 K. For a recent molecular beam study by Casavecchia[64−66] at a collision energy of 12.9 kcal/mol, this ratio amounts to 43:57. It therefore appears that the overall effect of crossing is not overly sensitive to the internal energy of $^{\bullet}CH_2CH_2O^{\bullet}$, although further experimental studies over a wider temperature range are necessary to fully settle this question. In this work, we used the value of 45:55 for the ratio in our following calculations of the rate of the ISC crossing as well as of the overall product branching ratios. To estimate the rate of the ISC crossing of the chemically activated $^{\bullet}CH_2CH_2O^{\bullet}$ radical, we use kinetic Scheme 1 where k_{TP} and k_{SP} are the overall disappearance rates of triplet $^{\bullet}CH_2CH_2O^{\bullet}$ on the triplet surface and of singlet $^{\bullet}CH_2CH_2O^{\bullet}$ on the singlet surface, respectively; $k_{f,ISC}$ and $k_{r,ISC}$ are the forward and reverse rates of ISC crossing, respectively. At or near room temperature, we have $k_{TP} \approx 1.3 \times 10^{11}$ s^{-1} (see above) whereas k_{SP} is found to be very high, $\approx 2.7 \times 10^{13}$ s^{-1} (see Appendix in Supporting Information). Although this k_{SP} value may be imprecise, its large magnitude shows that all singlet adducts, once formed, immediately evolve into further intermediates (CH_3CHO etc.), i.e., that $k_{SP} \gg k_{r,ISC}$, and hence that the rate of product formation through the singlet adduct is equal to the rate $k_{f,ISC}$ of the triplet → singlet ISC. It then also follows that $k_{TP}/k_{f,ISC} \approx$ triplet yields/singlet yields = 0.45:0.55, which leads to $k_{f,ISC} \approx 1.6 \times 10^{11}$ s^{-1} for the chemically activated radical with internal energy content of roughly 30−40 kcal/mol.

The results obtained for the overall product branching ratios are tabulated in Table 7 and plotted in Figure 4. Figure 4 shows

TABLE 6: Computed Primary Products Distribution (%) Evolving from the Singlet $^•CH_2CH_2O^•$ Biradical on the Singlet Surface under Various Reaction Conditions

T (K)	P (Torr)	$CH_3 + CHO$	$CH_3CO + H$	$CH_2CHO + H$	$H_2 + H_2CCO$	$CH_4 + CO$
287	5	86.5	4.1	0.7	4.4	4.3
	760	86.9	4.0	0.6	4.3	4.2
298	5	86.5	4.1	0.7	4.4	4.3
	760	86.8	4.1	0.6	4.3	4.2
500	5	85.2	4.6	0.9	4.7	4.6
	760	85.4	4.6	0.8	4.7	4.5
607	5	84.3	5.0	1.0	5.0	4.7
	760	84.5	4.9	1.0	4.9	4.7
1000	5	80.1	6.4	1.8	6.1	5.6
	760	80.1	6.4	1.8	6.1	5.6
1500	5	73.6	8.5	3.4	7.9	6.6
	760	73.6	8.5	3.4	7.9	6.6
2000	5	67.1	10.5	5.2	9.9	7.3
	760	67.1	10.5	5.2	9.9	7.3

TABLE 7: Computed Overall Primary Products Distribution (%) as a Function of Temperature Using the Value of 45:55 for the Ratio of Triplet and Singlet Yields; Where Possible, Experimental Data Are Also Given in Parentheses

T (K)	$H + CH_2CHO$	$CH_2(X^3B_1) + H_2CO$	$CH_3 + CHO$	$CH_3CO + H$	$H_2 + H_2CCO$	$CH_4 + CO$
287	40.3	5.1	47.8	2.2	2.4	2.3
	(39 ± 10)[a]	(10 ± 5)	(46 ± 10)		(5)	
298	40.1	5.2	47.7	2.2	2.4	2.3
	(40 ± 10)[b]	(10 ± 5)	(50 ± 10)			
500	37.1	8.3	47.0	2.5	2.6	2.5
607	35.2	10.3	46.4	2.7	2.7	2.6
	(38 ± 10)[a]	(13 ± 5)	(44 ± 10)		(5)	
1000	28.0	17.8	44.1	3.5	3.4	3.1
1500	21.7	24.8	40.5	4.7	4.3	3.6
2000	18.5	29.1	36.9	5.7	5.4	4.0

[a] Ref 23. [b] Ref 24.

SCHEME 1

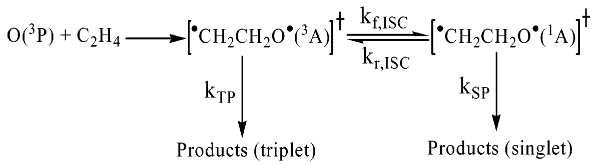

that the yield of $CH_2(X^3B_1) + H_2CO$ rapidly increases with increasing temperatures and should dominate at 2000 K. At the same time, the yields of $CH_3 + CHO$ and $H + CH_2CHO$ decrease, but they are the most important products at low temperatures. Other products, such as $H + CH_3CO$, $H_2 + H_2CCO$, and $CH_4 + CO$, are rather minor (≤5%) and slightly dependent on temperature over the wide range considered. At temperatures in the range 290−600 K, where experimental data are available, our computed detailed product distribution values are in excellent agreement with the experimental results (see Table 7) and lie within the experimental error bar. At room temperature and at low-to-atmospheric pressures, we would recommend the following product branching ratios: 40 ± 5% for $H + CH_2CHO$, 5 ± 3% for $CH_2(X^3B_1) + H_2CO$, 48 ± 5% for $CH_3 + CHO$, 2% for $CH_3CO + H$, 2.5% for $H_2 + H_2CCO$, and 2.5% for $CH_4 + CO$. The error bar for the computed results was evaluated by shifting **TS3** down 1 kcal/mol and **TS4** up 1 kcal/mol on the triplet energy surface.

Under Collision-Free Conditions. Let us first compare our computed primary product distribution with those recently observed in a molecular beam study by Casavecchia and co-workers.[64−66] This experiment was carried out at a collision energy of 12.9 kcal/mol. We assume here that this collision energy is converted to additional internal vibration energy of the initially formed triplet biradical adduct $^•CH_2CH_2O^•$. Note that a similar average thermal energy of the reactants is acquired at a temperature of about 1000 K. Microcanonical rate constants for various channels in the $O(^3P) + C_2H_4$ reaction computed at an internal energy of 12.9 kcal/mol above the initial reactants are tabulated in Table 8. We used the value of 45:55 for the ratio of the triplet yields over the singlet yields as above. Our computed values are as follows (the experimental data[64−66] are given in parentheses, also see Table S10 in Supporting Information): 28% (27 ± 6%) for $H + CH_2CHO$, 18% (16 ± 8%) for $CH_2(X^3B_1) + H_2CO$, 44% (43 ± 11%) for $CH_3 + CHO$, 3.5% (1 ± 0.5%) for $CH_3CO + H$, 3.5% (13 ± 3%) for $H_2 + H_2CCO$, and 3% for $CH_4 + CO$. Note that these values differ only marginally from the yields calculated for the thermal reaction at 1000 K. Our computed yields for the three most important channels agree well with those observed experimentally[64−66] except for the ketene + H_2 product channel. According to our theoretical results, $H_2 + H_2CCO$ are formed from the activated singlets CH_3COH and CH_3CHO, in competition mainly with dissociation of the latter to $CH_3 + CHO$, in a ratio of about 1:13. The experimental ratio however is 1:3.3. The reason for this discrepancy is not clear. Nonstatistical effects on the relative rates are unlikely, as the lifetime of the activated CH_3COH and CH_3CHO is ≈10 ps (see Table 8), which should suffice for ergodicity. Neither can centrifugal effects of high-J initial adducts explain this, as these should favor dissociation to $CH_3 + CHO$ through the loose variational TS much more than the four-center rearrangement/fragmentation to $H_2CCO + H_2$ through the tight **TS20**.

It is also of importance to evaluate the effect of collision energy (E_{col}) on the products distribution. For this purpose, we have computed product branching ratios at E_{col} = 6 kcal/mol (see Table 8), as used in a previous molecular beam study.[19] Our computed values as a function of the ratio of triplet over singlet yields are given in Table S11 (see Supporting Information). Again taking a triplet/singlet ratio of 45:55, the yield of $H + CH_2CHO$ considerably drops as a function of internal

TABLE 8: Calculated Microcanonical Rate Constants (s^{-1}) under Collision-Free Conditions ($P \approx 0$ atm) in the Molecular Beam Experiment for Initial Collision Energies E_{Col} of 6.0 and 12.9 Kcal/Mol

reaction channel	$k(E)/s^{-1}$	
	$E_{col} = 6.0$	$E_{col} = 12.9$
$^{\circ}CH_2{-}CH_2{-}O^{\circ}(^3A)$ (Int1a) → TS3 → $H_2CCHO(X^2A'') + H^{\circ}(X^2S)$	2.35×10^{11}	6.05×10^{11}
$^{\circ}CH_2{-}CH_2{-}O^{\circ}(^3A)$ (Int1a) → TS4 → $CH_2(X^3B_1) + H_2CO(X^1A_1)$	6.29×10^{10}	4.13×10^{11}
$^{\circ}CH_2{-}CH_2{-}O^{\circ}(^3A)$ (Int1a) → TS5 → $CH_3CHO(^3A)$ (Int2)	0.0	2.37×10^{8}
$^{\circ}CH_2{-}CH_2{-}O^{\circ}(^3A)$ (Int1a) → TS6 → $CH_2CHOH(^3A)$ (Int3)	3.46×10^{7}	1.27×10^{9}
$^{\circ}CH_2{-}CH_2{-}O^{\circ}(^1A)$ (Int4) → TS10 → $CH_3CHO(X^1A')$ (Int5)	1.46×10^{13}	1.38×10^{13}
$CH_3CHO(X^1A')$ (Int5) → TS10 → $^{\circ}CH_2{-}CH_2{-}O^{\circ}(^1A)$ (Int4)	4.46×10^{8}	1.08×10^{9}
$^{\circ}CH_2{-}CH_2{-}O^{\circ}(^1A)$ (Int4) → TS11 → $c{-}C_2H_4O(X^1A_1)$ (Int6)	3.83×10^{12}	3.99×10^{12}
$c{-}C_2H_4O(X^1A_1)$ (Int6) → TS11 → $^{\circ}CH_2{-}CH_2{-}O^{\circ}(^1A)$ (Int4)	9.23×10^{9}	2.15×10^{10}
$^{\circ}CH_2{-}CH_2{-}O^{\circ}(^1A)$ (Int4) → TS12 → $CH_2CHOH(X^1A')$ (Int7a)	9.07×10^{12}	9.31×10^{12}
$CH_2CHOH(X^1A')$ (Int6a) → TS12 → $^{\circ}CH_2{-}CH_2{-}O^{\circ}(^1A)$ (Int3)	4.39×10^{8}	1.10×10^{9}
$CH_3CHO(X^1A')$ (Int5) → TS13 → $c{-}C_2H_4O(X^1A_1)$ (Int6)	1.27×10^{8}	3.39×10^{8}
$c{-}C_2H_4O(X^1A_1)$ (Int6) → TS13 → $CH_3CHO(X^1A')$ (Int5)	2.01×10^{10}	4.68×10^{10}
$CH_3CHO(X^1A')$ (Int5) → TS14 → $CH_2CHOH(X^1A')$ (Int7a)	6.38×10^{9}	1.15×10^{10}
$CH_2CHOH(X^1A')$ (Int7a) → TS14 → $CH_3CHO(X^1A')$ (Int5)	1.01×10^{10}	1.73×10^{10}
$CH_3CHO(X^1A')$ (Int5) → TS15 → $CH_3COH(X^1A)$ (Int8a)	1.08×10^{9}	2.50×10^{9}
$CH_3COH(X^1A)$ (Int8a) → TS15 → $CH_3CHO(X^1A')$ (Int5)	1.88×10^{11}	3.09×10^{11}
$CH_2CHOH(X^1A')$ (Int7a) → TS16 → $CH_3COH(X^1A)$ (Int8a)	3.19×10^{9}	6.11×10^{9}
$CH_3COH(X^1A)$ (Int8a) → TS16 → $CH_2CHOH(X^1A')$ (Int7a)	3.51×10^{11}	5.02×10^{11}
$c{-}C_2H_4O(X^1A_1)$ (Int6) → TS22 → $CH_2CHOH(X^1A')$ (Int7a)	5.52×10^{8}	1.99×10^{9}
$CH_2CHOH(X^1A')$ (Int7a) → TS22 → $c{-}C_2H_4O(X^1A_1)$ (Int6)	5.53×10^{6}	2.18×10^{7}
$CH_3CHO(X^1A')$ (Int5) → TS17 → $^{\circ}CH_3(X^2A_2'') + ^{\circ}CHO(X^2A')$	2.75×10^{10}	5.77×10^{10}
$CH_3CHO(X^1A')$ (Int5) → TS18 → $CH_3C^{\circ}O(X^2A') + H^{\circ}(X^2S)$	1.55×10^{9}	4.50×10^{9}
$CH_3CHO(X^1A')$ (Int5) → TS19 → $CH_2CHO(X^2A'') + H^{\circ}(X^2S)$	2.93×10^{8}	1.17×10^{9}
$CH_3CHO(X^1A')$ (Int5) → TS20 → $CH_2CO(X^1A_1) + H_2(X^1\Sigma_g)$	8.03×10^{8}	1.98×10^{9}
$CH_3CHO(X^1A')$ (Int5) → TS21 → $CH_4(X^1A_1) + CO(X^1\Sigma^+)$	1.51×10^{9}	3.96×10^{9}
$CH_2CHOH(X^1A')$ (Int7a) → TS24 → $CH_2CO(X^1A_1) + H_2(X^1\Sigma_g)$	3.09×10^{7}	1.31×10^{8}
$CH_3COH(X^1A)$ (Int8a) → TS25 → $CH_2CO(X^1A_1) + H_2(X^1\Sigma_g)$	7.30×10^{10}	1.40×10^{11}

energy, from 36% at $E_{col} = 6$ kcal/mol to 28% at $E_{col} = 12.9$ kcal/mol, whereas the yield of $CH_2(X^3B_1) + H_2CO$ increases from 10% to 18%. The yield of $CH_3 + CHO$ is less dependent on internal energy.

III.3. Overall Thermal Rate Coefficient. The overall temperature-dependent rate coefficient $k(T)_{overall}$ for the $O(^3P) + C_2H_4$ reaction can be computed according to the following expression:

$$k(T)_{overall} = (1 - \gamma_{re}) \times k_{TST}(T) \tag{13}$$

where γ_{re} is the fraction of redissociation of the initial adducts back to the initial reactants, $O(^3P) + C_2H_4$, and $k_{TST}(T)$ is the rate coefficient derived from transition state theory. The value of γ_{re} is a function of pressure and temperature; at the conditions considered ($T = 287-2000$ K and $P \leq 760$ Torr), it is negligibly small ($\ll$1%, see Tables 5 and 6), such that $k(T)$ can be computed directly from the multistate transition state theory expression:[46−50]

$$k(T)_{overall} = k(T)_{TST} = \frac{k_B T}{h} \times \frac{Q^{\neq}_{TS1a}\exp(-E^{\neq}_{TS1a}/RT) + Q^{\neq}_{TS1b}\exp(-E^{\neq}_{TS1b}/RT)}{Q_O Q_{C_2H_4}} \tag{14}$$

where $Q(T)$ is a complete partition function, k_B Boltzmann's constant, h Planck's constant, R the universal gas constant, and $E^{\ddagger}_{TS1a}$ and $E^{\ddagger}_{TS1b}$ are the barrier heights of 1.3 and 2.6 kcal/mol (see Figure 1) for the initial addition channels, respectively. The rotational symmetries for C_2H_4 and the transition states are 4 and 1, respectively, such that the reaction path degeneracy is 4.

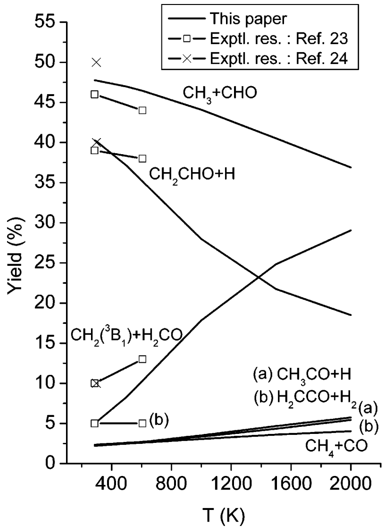

Figure 4. Primary products distribution for the $O(^3P) + C_2H_4$ reaction obtained at temperatures in the range of 287−2000K and $P = 760$ Torr using the value of 45:55 for the ratio of triplet and singlet yields.

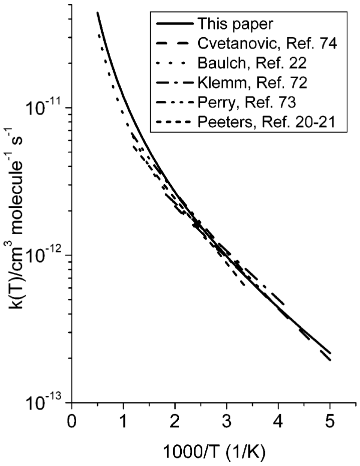

Figure 5. Overall thermal rate coefficients computed (TST) at temperatures in the range of 200−2000K. Experimental data are given for the purpose of comparison.

The electronic partition function of the O atom explicitly includes the three lowest-lying electronic states ($^3P_2$ with g-electronic degeneracy = 5, $^3P_1(g = 3)$, and $^3P_0(g = 1)$), with relative energies of 0.0000, 0.4525, and 0.6490 kcal/mol, respectively.[71] In addition, the electronic degeneracy of 3 for **TS1a** and **TS1b**, having a triplet electronic state, is also taken into account.

We have computed overall thermal rate coefficients in the wide range of temperatures 200−2000 K. These are plotted in Figure 5, together with some of the available experimental data for comparison. Figure 5 shows that our computed $k(T)$ compare favorably with experiment[20−22,72−74] over a wide range of temperatures. At room temperature, our computed rate constant of 7.3×10^{-13} cm^3 molecule-^{1} s^{-1} is in excellent agreement with a recently recommended value of 7.5×10^{-13} cm^3 molecule^{-1} s^{-1}.[22] Using our computed data, we fitted our $k(T)_{\text{overall}}$ to a modified Arrhenius expression as: $k(T) = 1.69 \times 10^{-16} \times T^{1.66} \times \exp(-331\ K/T)$.

IV. Conclusions

In the present theoretical study, both triplet and singlet potential energy surfaces characterizing the $O(^3P) + C_2H_4$ reaction are constructed uniformly using high levels of theory such as G3, CBS-QB3, G2M(CC,MP2), and MRCI. RRKM−master equation calculations to evaluate primary product distribution were then carried out using the exact stochastic simulation method. In addition, overall thermal rate coefficients were determined using conventional transition state theory. A number of important results emerge from this study and can be summarized as follows:

(i) The $O(^3P) + C_2H_4$ reaction is confirmed to occur via an electrophilic addition mechanism as the first reaction step.[7]

(ii) Our computed relative energies are in better agreement with available experimental data than previous theoretical results.

(iii) As a result, our product branching ratios agree well with those observed experimentally earlier at temperatures in the range of 287−607 K. At lower temperatures, the $CH_3 + CHO$ and $H + CH_2CHO$ are predicted to be major products, whereas at higher temperature, the $CH_2(X^3B_1) + H_2CO$ products become important. At room temperature and atmospheric pressure, product branching ratios recommended by us are 40 ± 5% for $H + CH_2CHO$, 5 ± 3% for $CH_2(X^3B_1) + H_2CO$, 48 ± 5% for $CH_3 + CHO$, 2% for $CH_3CO + H$, 2.5% for $H_2 + H_2CCO$, and 2.5% for $CH_4 + CO$.

(iv) The experimental products yields in combination with our theoretical predictions indicate a high rate of "hot" $^\bullet CH_2$-$CH_2O^\bullet$ triplet-to-singlet intersystem crossing of $\approx 1.6 \times 10^{11}$ s^{-1}.

(v) Our products distribution evaluated for collision-free conditions is in good agreement with that recently observed in the molecular beam experiment at a collision energy of 12.9 kcal/mol.[65]

(vi) Product yields at flame temperatures are predicted to differ greatly from room temperature, the most striking case being $CH_2 + H_2CO$, with yield increasing 6-fold over the 300−2000 K range.

(vii) Overall thermal rate coefficients computed at temperatures in the range of 200−2000 K are in good agreement with experimental data and can be fitted to a modified Arrhenius expression as $k(T) = 1.69 \times 10^{-16} \times T^{1.66} \times \exp(-331\ K/T)$.

Acknowledgment. T.L.N. thanks the KULeuven Research Council (BOF fund) for a PhD scholarship. The authors are indebted to the FWO-Vlaanderen and the KULeuven-Research Council for continuing financial support. L.V. is a postdoctoral fellow of the FWO-Vlaanderen. T.L.N. thanks Prof. P. Casavecchia for useful discussions.

Supporting Information Available: Optimized geometries, zero-point energies, total energies, relative energies, rotational constants, harmonic vibrational frequencies, and the most important configuration coefficients in a wave function are given. This material is available free of charge via the Internet at http://pubs.acs.org.

References and Notes

(1) Peeters J.; Vinckier C. *Proc. Combust. Inst.* **1974**, *15*, 969.
(2) Bhargava A.; Westmoreland P. R. *Combust. Flame* **1998**, *115*, 456.
(3) Lindstedt R. P.; Skevis G. *Proc. Combust. Inst.* **2000**, *28*, 1801.
(4) White J. N.; Gardiner W. C., Jr. *J. Phys. Chem.* **1979**, *83*, 562.
(5) Wilk R. D.; Cernansky N. P.; Pitz W. J.; Westbrook C. K., *Combust. Flame* **1989**, *77*, 145.
(6) Lindstedt R. P.; Maurice L. Q. *Combust. Sci. Technol.* **1995**, *107*, 317.
(7) Cvetanovic R. J.; Singleton D. L. *Rev. Chem. Intermed.* **1985**, *5*, 183.
(8) Cvetanovic R. J. *J. Chem. Phys.* **1955**, *23*, 1375.
(9) Cvetanovic R. J. *Can. J. Chem.* **1955**, *33*, 1684.
(10) Cvetanovic R. J. *J. Chem. Phys.* **1956**, *25*, 376.
(11) Cvetanovic R. J. *J. Chem. Phys.* **1959**, *30*, 19.
(12) Cvetanovic R. J. *J. Chem. Phys.* **1960**, *33*, 1063.
(13) Cvetanovic R. J. *J. Phys. Chem.* **1970**, *74*, 2730.
(14) Nicovich J. M.; Ravishankara A. R. *Symp. Int. Combust. Proc.* **1982**, *19*, 23.
(15) Melius C. F. unpublished, see ref 19.
(16) Jursic B. S. *THEOCHEM* **1999**, *492*, 85.
(17) Hawkins M.; Andrews L. *J. Am. Chem. Soc.* **1983**, *105*, 2528.
(18) Bley U.; Dransfeld P.; Himme B.; Koch M.; Temps F.; Wagner H. Gc. *Symp. Int. Combust.* **1988**, *22*, 997.
(19) Schmoltner A. M.; Chu P. M.; Brudzynski R. J.; Lee Y. T., *J. Chem. Phys.* **1989**, *91*, 6926.
(20) Fonderie V.; Maes D.; Peeters J. *Bull. Soc. Chim. Belg.* **1983**, *92*, 641.
(21) Fonderie V.; Maes D.; Peeters J. In *Phys. Chem. Behav. Atmos. Pollut., Proc. Eur. Symp., 3rd*, **1984**, 274; Versino, B., Angeletti, G. Eds.; Reidel Publishing Company: Dordrecht/Boston/Lancaster, 1984.
(22) Baulch D. L.; Cobos C. J.; Cox R. A.; Frank P.; Hayman G.; Just Th.; Kerr J. A.; Murrells T.; Pilling M. J.; Troe J.; Walker R. W.; Warnatz J. *J. Phys. Chem. Ref. Data* **1994**, *23*, 847.
(23) Peeters J.; Maes D., *Tenth International Symposium on Gas Kinetics*; University College of Swansea, July 1988; p A31.
(24) Endo Y.; Tsuchiya S.; Yamada C.; Hirota E.; Koda S. *J. Chem. Phys.* **1986**, *85*, 4446.
(25) From NIST web page: http://srdata.nist.gov/cccbdb/.
(26) Yamaguchi K.; Yabushita S.; Fueno T.; Kato S.; Morokuma K., *Chem. Phys. Lett.* **1980**, *70*, 27.
(27) Fueno T.; Takahara Y.; Yamaguchi K. *Chem. Phys. Lett.* **1990**, *167*, 291.
(28) Dupuis M.; Wendoloski J. J.; Takada T.; Lester W. A., Jr. *J. Chem. Phys.* **1982**, *76*, 481.
(29) Smith B. J.; Nguyen M. T.; Bouma W. J.; Radom L. *J. Am. Chem. Soc.* **1991**, *113*, 6452.
(30) Curtiss L. A.; Raghavachari K.; Redfern P. C.; Rassolov V.; Pople J. A. *J. Chem. Phys.* **1998**, *109*, 7764.
(31) Montgomery J. A., Jr.; Frisch M. J.; Ochterski J. W.; Petersson G. A. *J. Chem. Phys.* **1999**, *110*, 2822.
(32) Mebel A. M.; Morokuma K.; Lin M. C. *J. Chem. Phys.* **1995**, *103*, 7414.
(33) Werner H. J.; Knowles P. J. *J. Chem. Phys.* **1988**, *89*, 5803.
(34) Knowles P. J.; Werner H. J. *Chem. Phys. Lett.* **1988**, *145*, 514.
(35) Becke A. D. *J. Chem. Phys.* **1993**, *98*, 5648.
(36) Stevens P. J.; Devlin F. J.; Chablowski C. F.; Frisch M. J. *J. Phys. Chem.* **1994**, *98*, 11623.
(37) *EMSL Basis Set Library*, http://www.emsl.pnl.gov/forms/basisform.html.
(38) Werner H. J.; Knowles P. J. *J. Chem. Phys.* **1985**, *82*, 5053.
(39) Knowles P. J.; Werner H. J. *Chem. Phys. Lett.* **1985**, *115*, 259.
(40) Langhoff S. R.; Davidson E. R. *Int. J. Quantum Chem.* **1974**, *8*, 61.
(41) Werner H. J. *Mol. Phys.* **1996**, *89*, 645.
(42) Celani P.; Werner H. J. *J. Chem. Phys.* **2000**, *112*, 5546.

(43) Frisch, M. J.; Trucks, G. W.; Schlegel, H. B.; Scuseria, G. E.; Robb, M. A.; Cheeseman, J. R.; Montgomery, Jr., J. A.; Vreven, T.; Kudin, K. N.; Burant, J. C.; Millam, J. M.; Iyengar, S. S.; Tomasi, J.; Barone, V.; Mennucci, B.; Cossi, M.; Scalmani, G.; Rega, N.; Petersson, G. A.; Nakatsuji, H.; Hada, M.; Ehara, M.; Toyota, K.; Fukuda, R.; Hasegawa, J.; Ishida, M.; Nakajima, T.; Honda, Y.; Kitao, O.; Nakai, H.; Klene, M.; Li, X.; Knox, J. E.; Hratchian, H. P.; Cross, J. B.; Bakken, V.; Adamo, C.; Jaramillo, J.; Gomperts, R.; Stratmann, R. E.; Yazyev, O.; Austin, A. J.; Cammi, R.; Pomelli, C.; Ochterski, J. W.; Ayala, P. Y.; Morokuma, K.; Voth, G. A.; Salvador, P.; Dannenberg, J. J.; Zakrzewski, V. G.; Dapprich, S.; Daniels, A. D.; Strain, M. C.; Farkas, O.; Malick, D. K.; Rabuck, A. D.; Raghavachari, K.; Foresman, J. B.; Ortiz, J. V.; Cui, Q.; Baboul, A. G.; Clifford, S.; Cioslowski, J.; Stefanov, B. B.; Liu, G.; Liashenko, A.; Piskorz, P.; Komaromi, I.; Martin, R. L.; Fox, D. J.; Keith, T.; Al-Laham, M. A.; Peng, C. Y.; Nanayakkara, A.; Challacombe, M.; Gill, P. M. W.; Johnson, B.; Chen, W.; Wong, M. W.; Gonzalez, C.; Pople, J. A. *Gaussian 03*, Gaussian, Inc., Wallingford CT, 2004.

(44) Helgaker T.; Jensen H. J. Aa.; Joergensen P.; Olsen J.; Ruud K.; Aagren H.; Auer A. A. Bak, K. L.; Bakken, V.; Christiansen, O.; Coriani, S.; Dahle, P.; Dalskov, E. K.; Enevoldsen, T.; Fernandez, B.; Hättig, C.; Hald, K.; Halkier, A.; Heiberg, H.; Hettema, H.; Jonsson, D.; Kirpekar, S.; Kobayashi, R.; Koch, H.; Mikkelsen, K. V.; Norman, P.; Packer, M. J.; Pedersen, T. B.; Ruden, T. A.; Sanchez, A.; Saue, T.; Sauer, S. P. A.; Schimmelpfennig, B.; Sylvester-Hvid, K. O.; Taylor, P. R.; Vahtras, O. *DALTON: A Molecular Electronic Structure Program*, Release 1.2; 2001. See http://www.kjemi.uio.no/software/dalton/dalton.html.

(45) *MOLPRO* is a package of ab initio programs written by Werner H.-J.; Knowles P. J.; Schütz M.; Lindh R.; Celani P.; Korona T.; Rauhut G.; Manby F. R.; Amos R. D.; Bernhardsson A.; Berning A.; Cooper D. L.,; Deegan M. J. O.; Dobbyn A. J.; Eckert F. et al., 2002.

(46) Robinson P.; Holbrook K. *Unimolecular Reactions*; Wiley-Interscience: London, 1972.

(47) Forst W. *Theory of Unimolecular Reactions*; Academic Press: New York, 1973.

(48) Gilbert R. G.; Smith C. S. *Theory of Unimolecular and Recombination Reactions*; Blackwell Scientific, Oxford, 1990.

(49) Holbrook K.; Pilling M.; Robertson S. *Unimolecular Reactions*, 2nd ed.; Wiley: New York, 1996.

(50) Steinfeld J. I.; Francisco J. S.; Hase W. L. *Chemical Kinetics and Dynamics*; Prentice-Hall: Englewood Cliffs, NJ, 1999.

(51) Baer T.; Hase W. L. *Unimolecular Reaction Dynamics: Theory and Experiment*; Oxford University Press: Oxford, 1996.

(52) Light J. C.; Hamilton I. P.; Lill J. V. *J. Chem. Phys.* **1984**, *82*, 1400.

(53) Colbert D. T.; Miller W. H. *J. Chem. Phys.* **1992**, *96*, 1982.

(54) Knyazev V. D. *J. Phys. Chem. A* **1998**, *102*, 3916.

(55) Beyer T.; Swinehart D. F. *Comm. Assoc. Comput. Mach.* **1973**, *16*, 379.

(56) Stein S. E.; Rabinovitch B. S. *J. Chem. Phys.* **1973**, *58*, 2438.

(57) Hipper H.; Troe J.; Wendelken H. J. *J. Chem. Phys.* **1983**, *78*, 6709.

(58) Troe J. *J. Chem. Phys.* **1977**, *66*, 4745.

(59) Gillespie D. T. *J. Comput. Phys.* **1976**, *22*, 403.

(60) Gillespie D. T. *J. Phys. Chem.* **1977**, *81*, 2340.

(61) Gillespie D. T. *J. Comput. Phys.* **1978**, *28*, 395.

(62) Matsumoto M.; Nishimura T. *ACM Trans. Model. Comput. Simul.* **1998**, *8*, 3.

(63) Vereecken L.; Huyberechts G.; Peeters J. *J. Chem. Phys.* **1997**, *106*, 6564.

(64) Capozza G.; Segoloni E.; Volpi G. G.; Casavecchia P. *The 18th International Symposium on Gas Kinetics*, Bristol, U.K., 2004.

(65) Casavecchia P.; Capozza G.; Segoloni E.; Volpi G. G.; Segologi E.; Leonori F.; Balucani N.; Volpi G. G. *J. Phys. Chem. A* **2005**, *109*, 3527.

(66) Personal communication with Prof. P. Casavecchia.

(67) Westley F.; Herron J. T.; Cvetanovic R. J.; Hampson R. F.; Mallard W. G. *NIST Standard Reference Database 17,* Verson 3.0; National Institute of Standards and Technology: Gaithersburg, MD, 1991; p 20899.

(68) Malick D. K.; Petersson G. A.; Montgomery J. A., Jr. *J. Chem. Phys.* **1998**, *108*, 5704.

(69) Klein S.; Bearpark M. J.; Smith B. R.; Robb M. A.; Olivucci M.; Bernardi F. *Chem. Phys. Lett.* **1998**, *292*, 259.

(70) Liu, Y. P.; Lu, D. H.; Gonzalez-Lafont, A.; Truhlar, D. G.; Garrett, B. C. *J. Am. Chem. Soc.* **1993**, *115*, 7806 and see references therein.

(71) From NIST web page: http://physics.nist.gov/PhysRefData/Handbook/periodictable.htm.

(72) Klemm R. B.; Nesbitt F. L.; Skolnik E. G.; Lee J. H.; Smalley J. F. *J. Phys. Chem.* **1987**, *91*, 1574.

(73) Perry R. A. *J. Chem. Phys.* **1984**, *80*, 153.

(74) Cvetanovic R. J. *J. Phys. Chem. Ref. Data* **1987**, *16*, 261.

(75) Koda S.; Endo Y.; Tsuchiya S.; Hirota E. *J. Phys. Chem.* **1991**, *95*, 1241.

(76) Oguchi T.; Ishizaki A.; Kakuta Y.; Matsui H.; Miyoshi A. J. *J. Phys. Chem. A* **2004**, *108*, 1409 and see ref 14 therein.

(77) Herschbach D. R. *J. Chem. Phys.* **1959**, *31*, 91.